A Microgrid Monitoring System Over Mobile Platforms

Haoyang Lu, *Student Member, IEEE*, Lingwei Zhan, *Member, IEEE*, Yilu Liu, *Fellow, IEEE*, and Wei Gao, *Member, IEEE*

***Abstract*—Real-time awareness of the phasor state, including the volatile frequency and phase angle, is critical to maintain reliable and stable operations of the power grid. However, the high cost and low accessibility of current synchrophasors restrict their large-scale deployment over highly distributed microgrids. In this paper, we present a practical system design for monitoring the microgrid frequency and phase angle over mobile platforms and significantly reduce the cost of such monitoring. Being different from current synchrophasors, our system does not rely on continuous GPS reception and hence it is highly accessible and applicable to heterogeneous microgrid scenarios. We develop various techniques to provide the timing signal that is necessary for precise microgrid monitoring. For frequency monitoring, the network time protocol is exploited for time synchronization. For phase angle monitoring which requires a higher timing accuracy, 200 Hz primary synchronization signal being embedded in the 4G LTE cellular signal is harvested for time synchronization. We implemented our system over off-the-shelf smartphones with a few peripheral hardware components and realized an accuracy of 1.7 MHz and 0.01 rad for frequency and phase angle monitoring, respectively. Although the accuracy of the prototype is lower than that of the GPS-based systems, the system could still satisfy the requirements of microgrid monitoring. The total cost of the system can be controlled within $100 and no installation cost is required. Experiment results compared with the traditional frequency disturbance recorders verify the effectiveness of our proposed system.**

***Index Terms*—Smart grid, microgrid monitoring, network time protocol (NTP), primary synchronization signal (PSS), mobile platform.**

I. Introduction

MICROGRIDS, operating in either grid-connected mode or islanded mode, enable local integration of energy generation, distribution, and storage at the consumer level for better power system efficiency and control of demand [1]. To maintain the stable operation of microgrids, phasor states of both microgrid and the Area Electric Power System (AEPS) to which the microgrid connected, including frequency, phase angle, and voltage magnitude, should be monitored continuously, especially during the transition between two operation modes, i.e., resynchronization and islanding process [2].

Manuscript received February 5, 2015; revised June 8, 2015 and October 5, 2015; accepted December 4, 2015. Date of publication January 6, 2016; date of current version February 16, 2017. Paper no. TSG-00129-2015.

The authors are with the Department of Electrical Engineering and Computer Science, University of Tennessee, Knoxville, TN 37996 USA (e-mail: hlu9@utk.edu; lzhan@utk.edu; liu@utk.edu; weigao@utk.edu).

Color versions of one or more of the figures in this paper are available online at http://ieeexplore.ieee.org.

Digital Object Identifier 10.1109/TSG.2015.2510974

Current power grid monitoring systems allow direct measurement of frequency and phase angle by installing synchrophasors at either high-voltage transmission level [3] or low-voltage distribution level [4]. These power grid monitoring systems, although having been proved to be effective in wide-area power grid infrastructure, are generally considered unsatisfactory for monitoring the operating status of the newly emerging distributed power systems, so-called microgrids [5]. The decentralization of microgrids poses higher requirements on the installation cost and accessibility of power monitoring devices, and makes the current synchrophasors too expensive and inconvenient to be deployed into individual households in high volume. PMUs are deployed in substations and equipped with current transformer and power transformer for accessing the high voltage, which increases both manufacturing cost and the installation cost. For example, the installation cost of one transmission-level Phasor Measurement Unit (PMU) is more than $80,000 at the Tennessee Valley Authority (TVA). These PMUs are not intended to be used at the distributed consumer level, and require professional installation which reduces end-users' incentives of having synchrophasors in their home energy systems.

In this paper, we present a practical system design which bridges the gap between current power grid monitoring systems and the unique requirements of microgrid monitoring. Development of such a microgrid monitoring system, however, is challenging due to the requirements of microgrid monitoring on accurate time synchronization, high-resolution sensing, and real-time data processing. First, power grid operations should be monitored in real-time using globally synchronized timestamps, so that measurements from dispersed locations can be compared on a common time reference [6]. Although GPS signal that is widely used in current synchrophasors can provide a sub-microsecond timing accuracy, however, it has limited use for microgrids due to its deficiency for indoor scenarios. Second, with the increasing resolution and responsiveness of phasor state estimation, the workload of processing measurement data may exceed the computational capacity of current measurement devices. Specialized DSP chips are used in present synchrophasors for data processing, but are difficult and too expensive to be integrated into microgrid monitoring systems which need to be deployed in high volume.

Our main idea to overcome the aforementioned challenges is to reduce the systematic cost of frequency and phase angle monitoring by developing efficient embedded sensing platforms and adopting GPS-free time synchronization methods,

without impairing the accuracy of AC waveform measurement and phasor state estimation. To the best of our knowledge, we are the first to achieve high-precision wide-area power grid monitoring without GPS synchronization. Our detailed contributions are as follows:

- We implemented a low-cost microgrid monitoring system over the smartphone platform with a small quantity of peripheral hardware components. This prototype system can be further integrated into the smartphone charger for better flexibility and convenience.
- We proposed GPS-free frequency monitoring methods utilizing the Network Time Protocol (NTP), which significantly increases the system flexibility by eliminating the requirement of GPS reception and line of sight to the satellites.
- We extended the frequency monitoring prototype to further implement the functionality of phase angle monitoring by harvesting the Primary Synchronization Signal (PSS) in the 4G LTE cellular signal for time synchronization.
- We proposed adaptive frequency estimation algorithm to reduce the computational load of data processing at smartphones.

The rest of this paper is organized as follows. Section II discusses the background knowledge of power grid monitoring and the related work. Section III provides an overview of our system design. Section IV introduces the adaptive frequency estimation algorithm and the NTP-based frequency monitoring design. Section V presents the LTE-based phase angle monitoring design. Section VI presents our performance evaluation results in comparison with FDRs. Section VII presents the discussion. Finally, the conclusions and future work are drawn in Section VIII.

II. Background and Related Work

The power grid frequency and phase angle are generally measured from samples of the voltage waveform. Several algorithms such as curve-fitting method [7], [8], Kalman filter-based methods [9], and DFT-based algorithms [10], [11] have been proposed for such measurement.

Built on these measurement algorithms, wide-area power grid monitoring systems have been established via deployment of PMUs in the transmission level. Synchrophasors such as Frequency Disturbance Recorders (FDRs) [12] and micro-PMUs (μPMU) [13], on the other hand, are deployed in the distribution level with a greatly reduced monitoring cost. Specifically, based on FDRs, a worldwide Frequency monitoring NETwork (FNET) has been designed and deployed [14], enabling many applications of power system monitoring, control, and management, such as abnormal events detection and location.

Synchronization among different synchrophasors is important for wide-area power system monitoring. To achieve this, the Pulse-Per-Second (PPS)[1] signal being retrieved from GPS receivers is generally used as the synchronization signal [15]. The PPS signal is an analog output signal with a rising edge at each one second boundary of the Universal Coordinated Time (UTC). Since the precision of GPS signal is in nanoseconds with non-accumulative time drift [16], synchrophasors at dispersed locations can measure local system state synchronously through the integrated GPS clock.

[1]In the rest of the paper, we will use the terms "GPS signal" and "PPS signal" interchangeably.

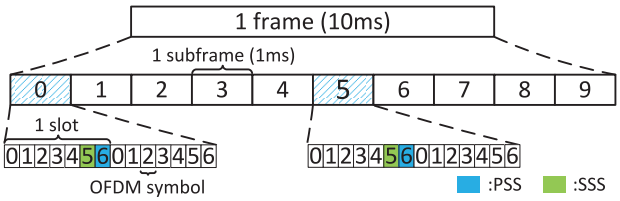

Fig. 1. Synchronization signals in LTE FDD downlink.

For better accessibility and lower cost, less expensive yet accurate timing sources have been studied in recent years. A NTP-synchronized Wide Area Frequency Measurement System (WAFMeS) has been implemented [17] and is able to detect the large swing disturbance at the granularity of 0.2 Hz. However, its flexibility and accessibility is restricted, and its accuracy of frequency estimation is too low to be applied to the U.S. power grid with much higher stability and smaller disturbances. Extensive researches have also been done on harvesting the timing information from the GSM cellular communication system [18]. More specifically, the 21 Hz Frequency Correction Burst (FCB), which is modulated at a frequency higher than the main carrier frequency, is harvested from the main carrier through development of 0.13μm CMOS fabrication techniques. Since the GSM base stations are strictly synchronized to a single timing source with an accuracy better than 0.05 microseconds [19], GSM signal is able to achieve an equivalent timing accuracy as the GPS signal.

III. Overview

In this section, we first discuss our motivation of exploiting GPS-free time synchronization methods for microgrid monitoring. Specifically, we adopt Network Time Protocol (NTP) for frequency monitoring, and LTE synchronization signals for phase angle monitoring. Afterwards, we present the hardware and software designs of our power grid monitoring system.

A. Motivation

1) Motivation for NTP-Based Frequency Monitoring: Network Time Protocol (NTP) [20] is being widely used in current computing systems, such as the Windows Time Service, in order to synchronize the local clock of digital devices with UTC. Due to the uncertainty of network transmission delay, the timing accuracy of NTP is in the order of 10 milliseconds [21] and is much lower than that of the GPS signal. Nevertheless, by investigating the sample events in the power grid [22] that are recorded by FNET (see Section VII-A), we found that such time precision is sufficient for detecting a frequency disturbance event. Therefore, the NTP is an appropriate alternative to provide global time synchronization to frequency measurement data, replacing the

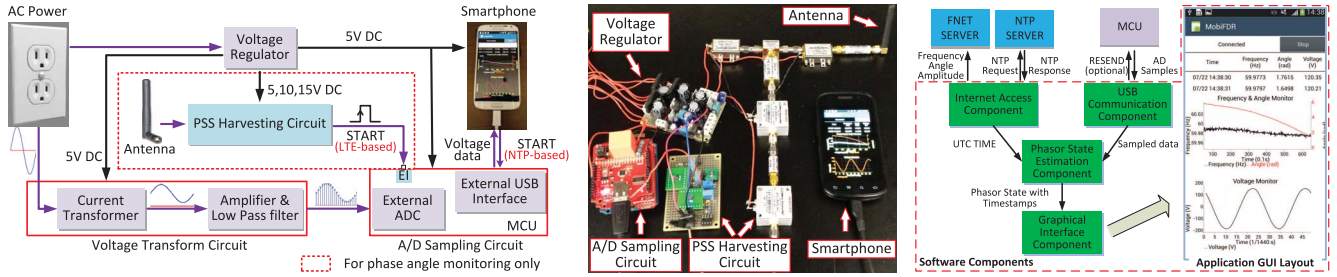

(a) System design (b) System implementation (c) Software components in the Android application

Fig. 2. Power grid monitoring over smartphones.

GPS signal. Being different from the GPS signal which continuously feeds the processor, the NTP timing information is only available when the monitoring device sends a request to the remote NTP server. The uncertainty of such round-trip network transmission delay, therefore, further complicates the design of time synchronization method.

2) Motivation for LTE-Based Phase Angle Monitoring: Compared to frequency monitoring, phase angle monitoring requires a globally synchronized clock with higher accuracy and stability. Simply speaking, a 15-millisecond timing error, which is usually the upper bound of NTP timing error, corresponds to an unacceptable phase angle measurement error of 5.76 radians in a 60 Hz power system. Instead, we propose to harvest the precise timing signal from the 4G LTE cellular signal, which is widely available nationwide nowadays. The enhanced base station (eNodeB) of LTE is strictly synchronized with GPS or the Precision Time Protocol (PTP) [23]. The cell ID in the LTE network is defined within two synchronization signals, namely Primary Synchronization Signal (PSS) and the Secondary Synchronization Signal (SSS). Fig. 1 illustrates the LTE frame format and the location of synchronization signals under Frequency-Division Duplexing (FDD) mode. The PSS repeats periodically (every 5 ms) and therefore can be regarded as a time synchronization signal.

B. Hardware Design

Our monitoring system consists of a voltage regulator module, a voltage transform circuit, a microprocessor-based analog-to-digital (AD) sampling module and an Android-based smartphone. The system design and implementation are shown in Fig. 2(a) and 2(b), respectively. The voltage regulator outputs the necessary DC power to power up the whole system, including the smartphone. An 8-bit microprocessor (MCU) ATmega328 (Arduino Uno board) is used to control the voltage sampling process through external AD Converter (ADC) at the sampling frequency of 1,440 Hz, and sends these raw voltage data to smartphone every 100 ms for phasor state estimation processing. The communication between the microprocessor and the smartphone is conducted by the USB host controller IC MAX3421E (USB host shield) [24]. Similar as being connected to the desktop PC, the smartphone behaves as USB slave in relation to the USB host chip, and can communicate with the MCU and be charged at the meantime.

The PSS harvesting circuit, shown within the dotted line in Fig. 2(a), will be attached to the frequency monitoring system for phase angle monitoring. In the LTE-based phase angle monitoring, the PSS harvesting circuit will extract the PSS signals and transmit them to the MCU in the form of pulses. The rising edges of the pulses will be detected through External Interrupt (EI) in the MCU, and trigger new sampling cycles. The PSS harvesting circuit will be illustrated in detail in Section V.

C. Software Design

As shown in Fig. 2(c), we developed an Android application to process the measurement data at the smartphone and visually display the monitoring results to users. To ensure prompt processing of measurement data, each computationally intensive operation, including the phasor state estimation and NTP request and response, is processed by a separate software thread instead of residing in the application main thread. Our application consists of four major components:

1) *USB Communication Component:* Through USB connection, the MCU-based AD sampling module uploads the waveform samples onto the smartphone for processing. The smartphone will respond with RESEND command if error exists during the data transfer. In the NTP-based frequency monitoring, a new sampling cycle starts once MCU receives trigger from the smartphone. Our application will also monitor the connection status of the USB accessory, and run automatically when a correct hardware signature is connected.
2) *Internet Access Component:* Network access is necessary to obtain the NTP timing information. The UTC timestamp is retrieved by requesting the NTP server. In addition, the measurement information will be uploaded via the Internet to FNET servers hosted in the University of Tennessee.
3) *Phasor State Estimation Component:* The phasor-based frequency estimation algorithm described in Section IV-A is implemented in this component. The MCU will store the sampled data within the last 100 ms and send them to the smartphone at one time. Once these 144 samples are received by the smartphone, our application would estimate the operating frequency from these samples. In addition, the phase angle of the first sample will be selected as the phase angle output in this period.
4) *Graphic Interface Component:* The information of frequency, phase angle and voltage amplitude of the AC

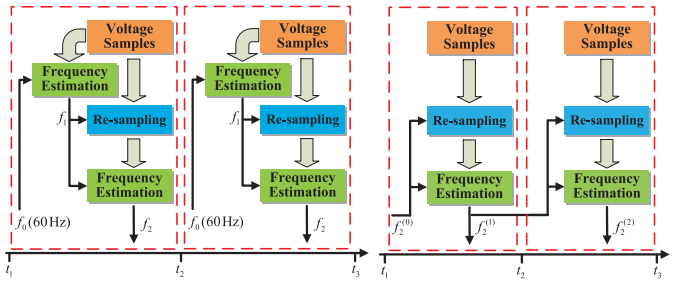

(a) Original algorithm (b) Adaptive algorithm

Fig. 3. Frequency estimation algorithms.

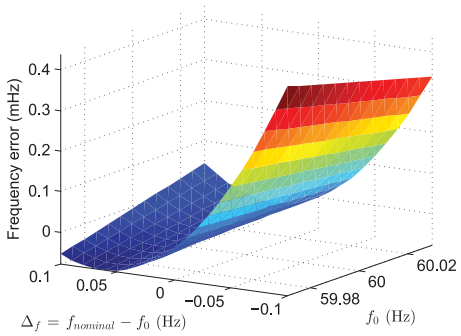

Fig. 4. Frequency measurement error under 60 dB AWGN.

waveform are displayed at the screen for better user interaction.

IV. Frequency Monitoring

Compared to the widely-used DSP chips in current synchrophasors, mobile platforms such as smartphones are not specialized for, and may be overloaded by real-time computation over voltage waveform samples, especially under the condition of heavy workload. In addition, more powerful smartphones usually mean higher cost, which is contradictory to our motivation of low-cost monitoring. Therefore, the reduction of computational workload is highly important, especially under high sampling frequency. In this section, the adaptive frequency estimation algorithm is developed to reduce the computation load at smartphone. Afterwards, the operating frequency in the microgrid will be estimated based on the timing information from NTP.

A. Adaptive Frequency Estimation Algorithm

DFT-based phasor and frequency estimation algorithm is widely applied in phasor measurement area. However, the traditional DFT-based algorithm requires the sampling rate to be integer multiples of the power grid frequency, which is not satisfied when the power grid frequency deviates from its nominal frequency at a fixed sampling rate. The nominal frequency in North America is 60 Hz, and a sampling rate of 1,440 Hz is used in FDRs. This violation, known as "spectrum leakage", will introduce estimation errors. To address this problem, "re-sampling" is proposed for FDRs [11]. The basic idea is to reconstruct a series of samples from the original voltage samples, so that the resampling rate of the new samples is close to integer multiples of the power grid frequency. The flowchart of the FDR algorithm is shown in Fig. 3(a). The power grid frequency f_1 is first coarsely estimated by the DFT-based approach. Then the "re-sampling" module takes the original voltage samples and regenerates a new series of samples with the help of f_1. Afterwards, a fine-level frequency estimation is conducted using the reconstructed samples, the result of which (f_2) is used as the final frequency result.

As depicted in Fig. 3(a), the frequency is estimated twice for each computation window, which is 0.1 s in current design. Our basic idea to reduce such computation workload is to exploit the correlation of voltage waveforms between adjacent computation windows, so as to eliminate the redundancy in frequency estimation. To be compatible with the FNET network, the reporting rate of our prototype is set to be 10 Hz. Since the frequency of the U.S. power grid usually changes slowly, it is highly possible that the frequency between two consecutive computation windows varies little. Under such circumstances, the frequency calculated in the current computation window can be used to re-sample the data in the following computation window, so that there will always be 24 samples per power grid frequency period.

The modified adaptive algorithm is shown in Fig. 3(b), in which the frequency result in one sampling cycle will be regarded as the initial frequency of the next computation window. Hence, frequency estimation only needs to be executed once based on re-sampled data. The final frequency will be calculated as:

$$f_2^{(n+1)} = f_2^{(n)} + \delta f^{(n+1)} \tag{1}$$

where $f_2^{(n)}$ is the frequency result in the n-th computation window, which will serve as the initial frequency in the $(n+1)$-th computation window, and $\delta f^{(n+1)}$ is the correction frequency.

It is expected that the closer between nominal frequency and actual frequency, the more accurate frequency estimation result can be achieved. Therefore, the frequency measurement error is modeled as $error = \phi(f_0, \Delta f)$, in which f_0 is the actual frequency and Δf is defined as the difference between nominal frequency and actual frequency.

According to [25], the ramp rates of frequency is between -1.0 Hz/s to $+1.0$ Hz/s, which corresponds to ± 0.1Hz with regard to the reporting rate of every 0.1s. We applied different nominal frequencies onto the waveform with fixed frequency contaminated 60 dB AWGN. The error of the adaptive frequency estimation method in relation to the difference between nominal frequency $f_{nominal}$ and the actual power grid frequency f_0 is depicted in Fig. 4. Error of the adaptive method is less than 0.04 mHz when the change of the frequency in consecutive cycles is ± 20 mHz, and it will decrease to smaller than 0.013 mHz when the change is less than 5 mHz.

B. Local Clock Calibration and Timestamp Calculation

We further exploit the timing information from NTP to calibrate the local clock and calculate the local timestamps, so as to ensure precise frequency estimation. The local clock

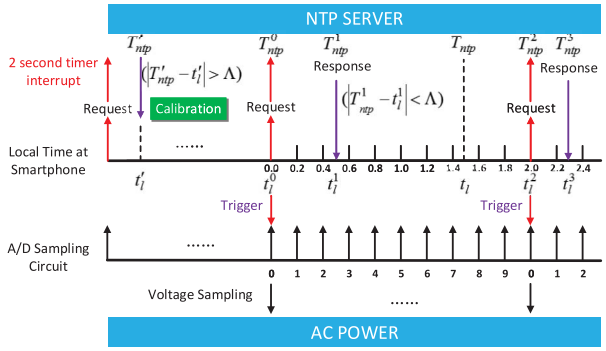

Fig. 5. Timestamps and time synchronization strategy.

of a smartphone will continuously drift due to the dynamic characteristics of the crystal oscillator, as well as various environmental factors such as temperature. As a result, the actual time period for each AC waveform sampling cycle may not be accurately set as expected. For example, a time period set to be 2000 ms by the smartphone may be actually 1998 ms or 2001 ms due to the local clock drift. Such inaccurate sampling frequency will result in the residue problem [26], i.e., the position of the first sample in one sampling cycle is different from that in another cycle, and the residue could be accumulated over time. To address this residue problem, our system starts a new sampling cycle every time when having sent out a NTP request, and hence guarantees the position of the first sample in each sampling cycle are the same in time. Correspondingly, the length of one sampling cycle is set to be 2 seconds, which is as twice as the period of the GPS signal. More frequent NTP requests than once every 4 seconds will be considered as attempting a Denial-of-Service (DoS) attack and hence denied by the NTP server [27]. Therefore, to avoid failures of NTP queries, the system will alternate the NTP servers to be requested so that one NTP server be requested from the system once within 10 seconds.

Each time when the smartphone triggers a sampling cycle, it calibrates its local clock using the received NTP timing information through comparison between the returned NTP timestamp T_{ntp} and the corresponding local time t_l. If $|T_{ntp} - t_l| > \Lambda$, which is the upper bound of NTP timing error, we will calibrate the local timer triggering the sampling cycle, i.e., using a new number rather than 2,000 milliseconds to setup the local timer for triggering the sampling cycles. More specifically, assuming that the local time of the most recent calibration in the past is t'_l and its corresponding NTP time is T'_{ntp}, the new setup time length V' for the local timer (in milliseconds) is defined as follows:

$$V' = \begin{cases} 2000 \cdot \left(t_l - t'_l\right) \Big/ \left(T_{ntp} - T'_{ntp}\right), & \text{if } |T_{ntp} - t_l| > \Lambda \\ V, & \text{Otherwise} \end{cases} \quad (2)$$

where V is the current setup value of the timer.

At the meantime, the local system time is also updated. For example, in Fig. 5, once receiving the NTP timing information and find that $|T'_{ntp} - t'_l| > \Lambda$, we change the local time from t'_l to T'_{ntp}.

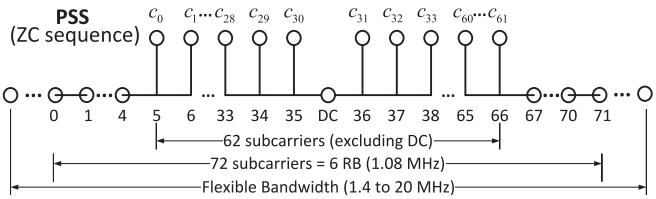

Fig. 6. Transmission of PSS signal in the frequency domain.

With NTP timing information, we recursively compute the timestamp of the current sampling cycle via proportional estimation from the previous cycle. We assume that the local clock drift within one sampling cycle is negligible. As a result, the timestamp of the first sample in one sampling cycle, which is also the start of the current sampling cycle, as well as the end of the previous sampling cycle, can be estimated from the NTP response and the corresponding local time. For example, in Fig. 5, the NTP time corresponding to t_l^2 can be estimated as:

$$T_{ntp}^2 = T_{ntp}^3 - \frac{t_l^3 - t_l^2}{t_l^3 - t_l^1} \cdot \left(T_{ntp}^3 - T_{ntp}^2\right). \quad (3)$$

V. Phase Angle Monitoring

As illustrated in Section III-A, measurement of phase angle requires more accurate timing information than the frequency monitoring does. In our system design, we aim to harvest synchronization signals from 4G LTE cellular signal for time synchronization as the substitution of GPS signal. Similar to the GPS-based system, the harvested LTE signal can be directly used to trigger a new sampling cycle.

A. PSS Harvesting Circuit Design

In LTE networks, to achieve high data transmission rate, Orthogonal Frequency Division Multiple Access (OFDMA) is utilized as the physical layer technique in the downlink data transmission [28]. The cell ID is represented as:

$$N_{ID}^{Cell} = 3N_{ID}^1 + N_{ID}^2 \quad (4)$$

where $N_{ID}^1 \in 0, 1, ..., 167$ is the cell identity group and is located in SSS signal, and $N_{ID}^2 \in 0, 1, 2$ is the cell identity and is located in PSS signal. The SSS signal indicates the frame timing as they are different within a frame, while PSS signal indicates the OFDM symbol timing as they are the same within a frame. The sequence used for the PSS is generated from a frequency domain Zadoff-Chu (ZC) sequence [29]:

$$c_u(n) = \begin{cases} e^{-j\frac{\pi un(n+1)}{63}} & n = 0, 1, ..., 30 \\ e^{-j\frac{\pi u(n+1)(n+2)}{63}} & n = 31, 32, ..., 61 \end{cases} \quad (5)$$

where the ZC root u for the PSS sequence is 25,29,34 that corresponds to the value of N_{ID}^2 = 0,1,2, respectively.

As shown in Fig. 6, comprised with three Zadoff-Chu sequences in frequency domain, the PSS signal maps to the central 62 subcarriers around DC (within the central six Resource Blocks (RBs)), enabling the frequency mapping of

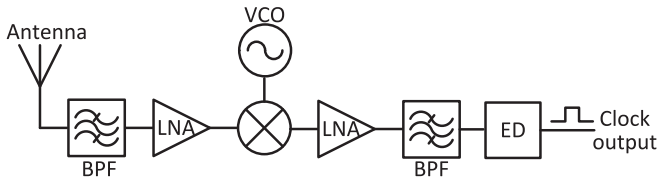

Fig. 7. System block diagram of the PSS signal harvesting circuit.

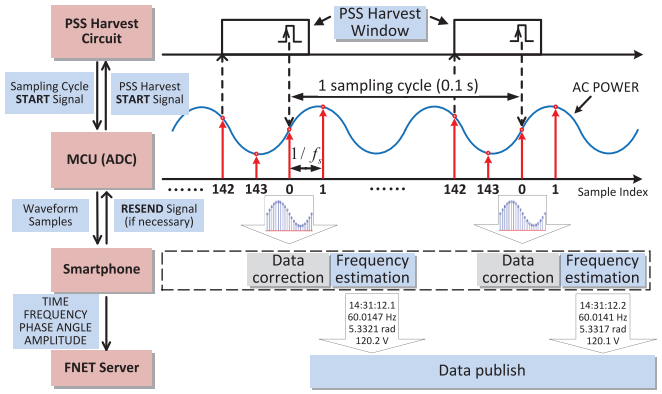

Fig. 8. System coordination between the smartphone and MCU.

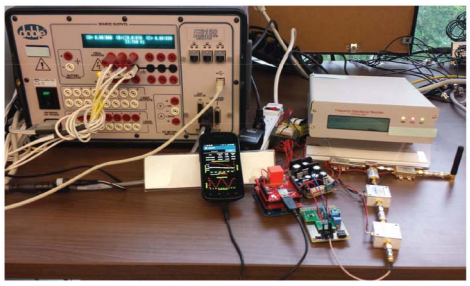

Fig. 9. Experiment setup.

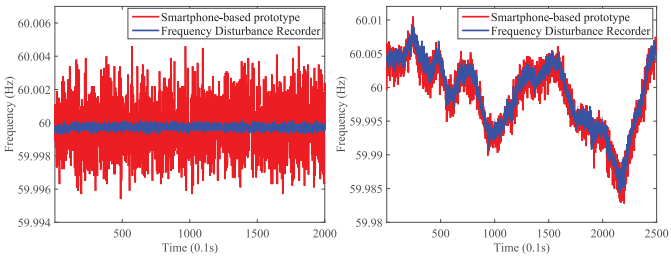

(a) 60 Hz constant output (b) 120 V wall power

Fig. 10. Frequency monitoring.

the synchronization signals to be invariant with respect to the system bandwidth, which varies from 1.4 MHz to 20 MHz.

Although PSS signal capturing is intrinsic to the LTE hardware within smartphones, the PSS detection is hidden from the IC chips and is inaccessible to the smartphone users, since the users are more concerned about the content of the radio frames, rather than when to receive the synchronization frames. Therefore we need to build our own PSS harvesting module. The frequency of PSS signal (200 Hz) is far lower than the bandwidth of data transmitted (in the order of 1 MHz). Since our purpose of PSS detection is not to decode the signal but only to identify the arrival of the PSS signals, the PSS signal can be detected based on the scheme shown in Fig. 7. A Voltage-Controlled Oscillator (VCO) is used to detect the frequency band with the strongest signal strength. The signal in 1900 MHz frequency band is selected and reduced to 200 kHz intermediate frequency (IF) output. The PSS signal would be transformed as a pulse after passing the bandpass filter with a bandwidth of 120 kHz and the envelope detector. The MCU will capture the rising edge of the PSS pulses as the trigger to start a new sampling cycle.

B. Coordination Between Smartphone and MCU

Our proposed method of determining the starting time of a new sampling cycle is shown in Fig. 8. Our monitoring system starts a new sampling cycle on every 100 ms for consistency with the reporting rate of the FNET network, and use 1,440 Hz as the sampling frequency to ensure the measurement accuracy (12 or more data samples per period is needed in a 60 Hz power system). Correspondingly, 144 data samples are recorded in each sampling cycle. To avoid false detection, we enable the PSS pulse detection only after the 142-nd samples (98.6 ms) is sampled in current sampling cycle. The pulse received in this period cycle is assumed to be the PSS signal tentatively, and the interval between the pulse and the last effective pulse is calculated. If the interval between them satisfies $\Delta t < \varepsilon$, then the pulse is considered as an effective PSS output. The detection window will be closed and a new sampling cycle starts immediately. Otherwise, the pulse is assumed to be noise and if no effective pulses are detected in the detection window, the MCU will start a new sampling cycle at the time when sampling the 144th samples. The phase angle of the first sample in each sampling period is obtained as the effective output in its corresponding period.

VI. Performance Evaluation

To evaluate the accuracy and effectiveness of frequency and phase angle monitoring of our proposed system, we test our system against the traditional FDR device. The system setup is shown in Fig. 9. The Doble F6150 power system simulator with GPS satellite synchronization is used to generate the standard AC power. The frequency and the phase angle accuracy of Doble F6150 simulator are 0.5 Part-Per-Million (PPM) and 0.1 degree respectively. Experiments over both standard power generator and regular AC wall power are conducted.

A. Frequency and Phase Angle Monitoring

The frequency measurement results over standard 60 Hz power generator and 120 V AC wall outlet are shown in Fig. 10. The error of the frequency measurement of our system under constant frequency waveform is 1.70 mHz, while that of the FDR device is 0.32 mHz. Under wall outlet measurement, our system is able to efficiently capture the trends of frequency deviations over time. Meanwhile, our system produces a 1.7 mHz difference from the FDR measurements being used as the reference. Currently, the frequency monitoring accuracy of our system is less than that of FDR due to

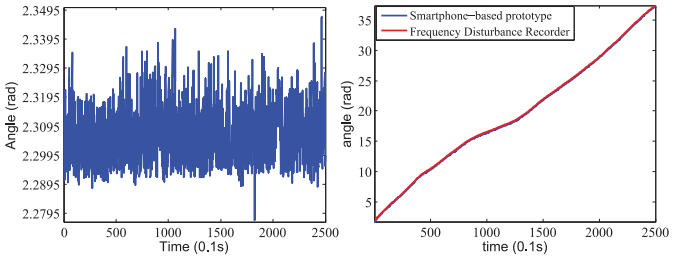

(a) 60 Hz constant output (b) 120 V wall power

Fig. 11. Phase angle monitoring.

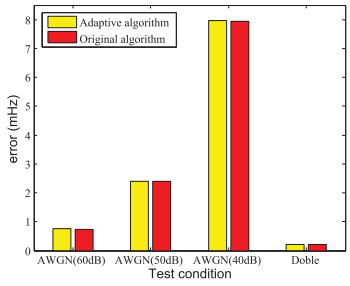

Fig. 12. Error of adaptive method over 60 Hz waveform.

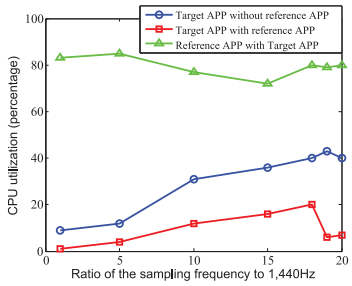

Fig. 13. CPU utilization via adaptive method.

a couple of reasons. Firstly, timing error exists in the timestamps compared to the real UTC time. That is, the time point of a frequency measurement may not be exactly aligned with its real timestamp. Secondly, to accommodate the data format of FNET and being able to integrate with NET framework, a curve fitting method is used to estimate the frequency points only at integral 100 millisecond points, such as 06:04:05.2, 06:04:05.3, etc, but may incur additional error due to the limited granularity of curve fitting. Thirdly, due to the involvement of both inductive and capacitive components such as current transformers and analog filters with different time constants, possible phase lag or advance may be introduced into the frequency monitoring. This may induce a constant time deviance between measurements of our system and the FDR. Fourthly, a 10-bit ADC is applied in our prototype compared to the 14-bit ADC used in FDRs, which is a contributor to the lower accuracy of our system.

For angle measurement, the standard deviation is used to evaluate the error under fixed-frequency condition. In the ideal condition, for waveform with fixed frequency, the curve of phase angle would be a line with fixed slope, in particular, a horizontal line under 60 Hz condition. The phase angle measurement results over standard 60 Hz power generator and 120 V AC wall outlet are shown in Fig. 11. The standard deviation of the phase angle measurement result is 0.01 rad under 60 Hz output, which corresponds to 32 us in 60 Hz system, compared to 0.0004 rad of the FDR device. In the experiment over wall power, since the PSS signal and the GPS signal are not precisely aligned, there is a nearly constant drift around the results. If eliminate the DC offset of two results, the difference between two curves is 0.011 rad.

Compared to FDR with an accuracy of 0.0004 rad, the timing error is mainly introduced in the PSS signal harvesting process. The PSS signals are harvested in the form of pulses, and then the rising edge of the pulses will be captured by the MCU through external interrupt. Compared to the GPS signal that in the form of pulses with a duration of 1.2 us and a steep rising edge, the slope of the rising edge of the PSS pulse is flatter and can be affected by the strength of the signal.

The existing design captures PSS signals through rising edge detection, which is completely achieved by analog components, and is constrained by the property of the MCU circuitry and of more uncertainty in a low SNR conditions. Therefore, a digital approach would further exploit the synchronization capability of PSS signals and is hence more suitable for PSS harvesting module. The specific implementation is to continuously collect the cellular signals through high-speed ADC, and to capture PSS signals through digital signal processing approach [30].

It is expected that there is a constant time offset between LTE PSS signals and GPS signals, which prevents the prototype being integrated into the GPS-based synchrophasor family. However, this problem could be addressed by manually compensating this time offset, which could be measured through GPS-disciplined instruments.

B. CPU Workload Reduction

The performance of our proposed adaptive frequency estimation method algorithm in Section IV-A is evaluated by both simulation and experiment. First, both the adaptive and the original methods are applied to the 60 Hz waveform contaminated with 60 dB, 50 dB and 40 dB AWGN. The error comparison between adaptive method and the original method is shown in Fig. 12. Under 40 dB AWGN, the error of the adaptive method is 7.96 mHz, which is 0.0157 mHz larger than that of the FDR. This error is slightly larger than that of the original methods and as the strength of noise decreases, the difference of the error between two methods is getting closer. The error decreases to 0.0015 mHz under 60 dB AWGN. Under the output of Doble, the difference of the error between two methods is 0.0001 mHz. Fig. 12 shows that the adaptive method can achieve an almost the same accuracy as the original algorithm under the same noise condition.

The CPU load test is conducted on the platform of smartphone Nexus S, which is equipped with a 512 MB memory and 1 GHz CPU clock. The smartphone is Android-based with the OS version 4.1.2. The CPU load of our application (referred to as target App) is tested under both idle and heavy load states. As a reference, a single-thread App (referred to as reference App) which operates a 60-by-60 matrix multiplication continuously is created. The reference App will consume 80% of the CPU load in the idle state. Fig. 13 shows the CPU load of

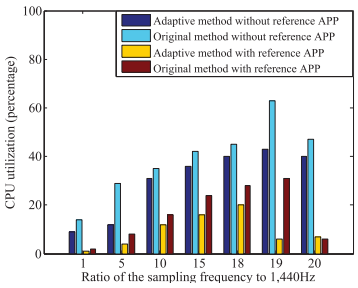

Fig. 14. CPU utilization comparison.

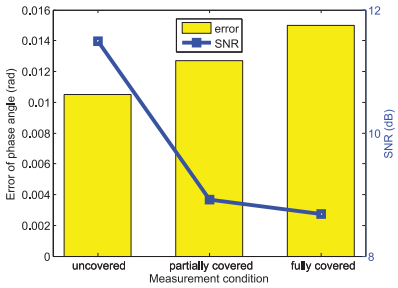

Fig. 15. Phase angle error under different SNR of PSS signal.

our application. In idle mode, the CPU load increases as the sampling frequency goes up since more samples need to be processed within 0.1 s. At the sampling frequency of 27,360 Hz ($19 \times 1,440$ Hz), the CPU load increases only 2% in idle mode and will decreases to 6% under the competition with reference App. Since the adaptive method is not parallel, and is implemented in a serialized manner (in a single thread), the CPU can't afford the serialization of the adaptive method in such a high sampling frequency. More computation resources will be distributed to the reference App.

The CPU utilization of the adaptive method compared to the original two-stage frequency estimation method is shown in Fig. 14. Since the computation in different sampling cycles is totally independent, the original algorithm can be achieved in a parallel style. However, the total amount of the computation keeps unchanged in both serialization and parallelization way, and it will consume more system resources to manage the multiple threads when executes parallel computing. Therefore, the original algorithm is also implemented in a serialization way. Under the idle state, the adaptive method will consume 4% less of the CPU load under the sampling frequency of 1,440 Hz. The CPU can't afford the serialization of the original algorithm in 27,360 Hz, which is the same as the adaptive method. The reason for this phenomenon is that the operations rather than the frequency estimation algorithm itself, such as the transmission of the large volume of the data, the correction of the received data, will consume large amount of computation resources, which cannot be neglected compared to the condition in a low sampling frequency. Fig. 12 and Fig. 14 demonstrate that the adaptive method could effectively reduce the CPU load with little accuracy loss compared to the original algorithm.

C. Measurement Accuracy vs. Signal-to-Noise Ratio

To evaluate the relationship between the measurement accuracy and the quality of the LTE cellular signal reception, we emulate the environment with different signal-to-noise ratio (SNR) by using aluminium foil to cover the antenna of the PSS harvesting antenna. The complete coverage of the foil onto the antenna corresponds to the worst SNR environment. The performance of the phase angle measurement with respect to different SNR is depicted in Fig. 15. From Fig. 15, the PSS harvesting module can achieve the highest SNR of 11.49 dB under no cover with the error of 0.01 rad on phase angle monitoring. As the coverage area of the foil increases, the error increases to 0.0127 and 0.015 rad in partially covered and totally covered situation, respectively. The reason of such a degradation partially results from the method of capturing the PSS pulses. That is, as the noise level increases, the voltage amplitude of the PSS signal become closer to that of the noises, which relates to a smooth rising edge of the PSS signal and susceptible to the noise. Since we regard the incoming of the rising edge of the PSS signal as the synchronization signal, the physical property of the MCU will introduce more uncertainty in a low SNR condition.

VII. Discussion

A. Discussion of NTP Timing Errors on Frequency Estimation

We investigated the sample event recorded by FNET [22] to show that a 10 ms accuracy is capable for power grid frequency monitoring.

The frequency estimation error caused by the NTP timing error can be represented as

$$f_e = t_e f' \tag{6}$$

where t_e is the NTP timing error in second, and f' is the Rate of Change of Frequency (ROCOF).

For a 1,800 MW generation trip event in Eastern Interconnection with a time span of 5 seconds, the grid frequency drops from 59.990 Hz to 59.895 Hz during this period. The ROCOF during this event can be calculated by $f' = (59.990 - 59.895)/5 = 0.019\ Hz/s$.

Given the NTP timing error of 10 millisecond, the frequency estimation error caused by the timing error during this event is given by $f_e = 0.01 f' = 0.19\ mHz$. We can see that this frequency estimation error is negligible, compared to the 5 mHz requirement in the PMU standard [25]. It should be noted that the frequency estimation error is much smaller when the power grid operates without events, when f' is close to zero.

B. Applications on Microgrid

A key use case of the prototype is the intentional islanding and re-synchronization of microgrids. These applications would require the comparison of phasors across the Point of Common Coupling (PCC). Although our device is dedicated for 120 V wall outlet, we can still measure the phase angle across the PCC by connecting a Potential Transformer (PT) between our device and PCC. The system accuracy is sufficient to support such operations, according to Table 5 in [2],

where a frequency accuracy of 0.1 Hz and phase angle accuracy of 0.1745 rad are required. In addition, if PCC is inaccessible, we can estimate the phase angle of PCC from the 120 V outlet with pre-known transformer structure. However, the accuracy of such an estimation needs further investigation. Though the system is expected to be deployed from behind the service transformer, the system is still suitable for some applications, such as abnormal event detection and location, which is based on detecting the variations of the phase angle difference between two locations.

VIII. Conclusion

In this paper, we presented the design and implementation of a GPS-free smartphone-based microgrid monitoring system. Specifically, we designed a simple NTP-based frequency monitoring prototype with a few peripherals. In addition, we harvested the PSS signal in the 4G LTE radio as the synchronization signal to achieve phase angle monitoring. The proposed adaptive method will reduce the computational load at the smartphone with nearly no accuracy loss. The experiments compared with FDR devices verify the effectiveness of the system on both frequency and phase angle monitoring. The systematic cost of the prototype excluding the smartphone is controlled within $100, and no specialized installation is required, which would facilitate the massive deployment of the monitoring system. Our future work will focus on further improving the performance of PSS harvesting module, simplifying the power grid monitoring system, and integrating more functionalities of power grid monitoring onto mobile platforms.

References

[1] F. Giraud and Z. M. Salameh, "Steady-state performance of a grid-connected rooftop hybrid wind-photovoltaic power system with battery storage," *IEEE Trans. Energy Convers.*, vol. 16, no. 1, pp. 1–7, Mar. 2001.

[2] *IEEE Guide for Monitoring, Information Exchange, and Control of Distributed Resources Interconnected With Electric Power Systems*, IEEE Standard 1547.3-2007, Nov. 2007.

[3] V. Venkatasubramanian, H. Schattler, and J. Zaborszky, "Fast time-varying phasor analysis in the balanced three-phase large electric power system," *IEEE Trans. Autom. Control*, vol. 40, no. 11, pp. 1975–1982, Nov. 1995.

[4] Y. Liu *et al.*, "Wide-area measurement system development at the distribution level: An FNET/GridEye example," *IEEE Trans. Power Del.*, Doi: 10.1109/TPWRD.2015.2478380.

[5] K. Tomsovic, D. E. Bakken, V. Venkatasubramanian, and A. Bose, "Designing the next generation of real-time control, communication, and computations for large power systems," *Proc. IEEE*, vol. 93, no. 5, pp. 965–979, May 2005.

[6] A. Armenia and J. H. Chow, "A flexible phasor data concentrator design leveraging existing software technologies," *IEEE Trans. Smart Grid*, vol. 1, no. 1, pp. 73–81, Jun. 2010.

[7] L. Zhan and Y. Liu, "Improved WLS-TF algorithm for dynamic synchronized angle and frequency estimation," in *Proc. IEEE PES Gen. Meeting Conf. Expo.*, National Harbor, MD, USA, Jul. 2014, pp. 1–5.

[8] W. Wang *et al.*, "Highly accurate frequency estimation for FNET," in *Proc. IEEE Power Energy Soc. Gen. Meeting (PES)*, Vancouver, BC, Canada, Jul. 2013, pp. 1–5.

[9] I. Kamwa, S. R. Samantaray, and G. Joos, "Compliance analysis of PMU algorithms and devices for wide-area stabilizing control of large power systems," *IEEE Trans. Power Syst.*, vol. 28, no. 2, pp. 1766–1778, May 2013.

[10] L. Zhan, Y. Liu, J. Culliss, J. Zhao, and Y. Liu, "Dynamic single-phase synchronized phase and frequency estimation at the distribution level," *IEEE Trans. Smart Grid*, vol. 6, no. 4, pp. 2013–2022, Jul. 2015.

[11] T. Xia, "Frequency monitoring network (FNET) algorithm improvements and application development," Ph.D. dissertation, Dept. Elect. Comput. Eng., Virginia Tech, Blacksburg, VA, USA, 2009.

[12] L. Wang *et al.*, "Frequency disturbance recorder design and developments," in *Proc. IEEE Power Eng. Soc. Gen. Meeting*, Tampa, FL, USA, 2007, pp. 1–7.

[13] A. Von Meier, D. Culler, A. McEachern, and R. Arghandeh, "Micro-synchrophasors for distribution systems," in *Proc. IEEE PES Innov. Smart Grid Technol. Conf. (ISGT)*, Washington, DC, USA, Feb. 2014, pp. 1–5.

[14] R. M. Gardner and Y. Liu, "FNET: A quickly deployable and economic system to monitor the electric grid," in *Proc. IEEE Conf. Technol. Homeland Security*, Woburn, MA, USA, 2007, pp. 209–214.

[15] A. G. Phadke, "Synchronized phasor measurements in power systems," *IEEE Comput. Appl. Power*, vol. 6, no. 2, pp. 10–15, Apr. 1993.

[16] C. Xu, "High accuracy real-time GPS synchronized frequency measurement device for wide-area power grid monitoring," Ph.D. dissertation, Dept. Elect. Comput. Eng., Virginia Polytech. Inst., Blacksburg, VA, USA, 2006.

[17] K. A. Salunkhe and A. Kulkarni, "A wide area synchronized frequency measurement system using network time protocol," in *Proc. 16th Nat. Power Syst. Conf.*, Hyderabad, India, 2010, pp. 266–271.

[18] J. K. Brown and D. D. Wentzloff, "A GSM-based clock-harvesting receiver with -87 dBm sensitivity for sensor network wake-up," *IEEE J. Solid-State Circuits*, vol. 48, no. 3, pp. 661–669, Mar. 2013.

[19] M. Mouly and M.-B. Pautet, *The GSM System for Mobile Communications*. Palaiseau, France: Telecom publishing, 1992.

[20] D. L. Mills, "Internet time synchronization: The network time protocol," *IEEE Trans. Commun.*, vol. 39, no. 10, pp. 1482–1493, Oct. 1991.

[21] L. Wang, J. Fernandez, J. Burgett, R. W. Conners, and Y. Liu, "An evaluation of network time protocol for clock synchronization in wide area measurements," in *Proc. IEEE Power Energy Soc. Gen. Meeting-Convers. Del. Elect. Energy 21st Cent.*, Pittsburgh, PA, USA, 2008, pp. 1–5.

[22] Power Information Technology Laboratory. *FNET Sample Events*. [Online]. Available: http://fnetpublic.utk.edu/sample_events.html, accessed May 6, 2015.

[23] *IEEE Standard for a Precision Clock Synchronization Protocol for Networked Measurement and Control Systems*, IEEE Standard 1588-2008 (Revision of IEEE Standard 1588-2002), Jul. 2008.

[24] *MAX3421E, USB Peripheral/Host Controller With SPI Interface*, Maxim Integrated Products, San Jose, CA, USA, 2007.

[25] *IEEE Standard for Synchrophasor Measurements for Power Systems*, IEEE Standard C37.118.1-2011 (Revision of IEEE Standard C37.118-2005), Dec. 2011.

[26] J. Zuo, "The frequency monitor network (FNET) design and situation awareness algorithm development," Ph.D. dissertation, Dept. Elect. Comput. Eng., Virginia Polytech. Inst. State Univ., Blacksburg, VA, USA, 2008.

[27] *NIST Internet Time Servers*. [Online]. Available: http://tf.nist.gov/tf-cgi/servers.cgi, accessed May 6, 2015.

[28] S. Sesia, I. Toufik, and M. Baker, *LTE: The UMTS Long Term Evolution*. Chichester, U.K: Wiley, 2009.

[29] 3rd Generation Partnership Project (3GPP), "Evolved universal terrestrial radio access (E-UTRA), physical channels and modulation (Release 10)," Version 10.0.0, ETSI, Sophia Antipolis, France, Tech. Rep. TS 36.211, 2010.

[30] W. Xu and K. Manolakis, "Robust synchronization for 3GPP LTE system," in *Proc. IEEE Glob. Telecommun. Conf. (GLOBECOM)*, Miami, FL, USA, Dec. 2010, pp. 1–5.

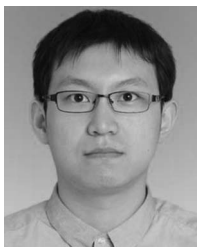

Haoyang Lu (S'15) received the B.E. degree from Hangzhou Dianzi University in 2010 and the M.E. degree from the University of Chinese Academy of Sciences in 2013, both in electrical engineering. He is currently pursuing the Ph.D. degree with the Department of Electrical Engineering and Computer Science, University of Tennessee, Knoxville. His research interests include smart grid and communication system.

Lingwei Zhan (S'13–M'15) received the B.S. and M.S. degrees in electrical engineering from Tongji University in 2008 and 2011, respectively, and the Ph.D. degree from the Department of Electrical Engineering and Computer Science, University of Tennessee, Knoxville, in 2015. He is currently with General Electric Grid Solutions, Philadelphia, PA, USA. His research interests include PMUs, synchrophasor measurement algorithms, embedded system development, wide-area power system monitoring, FACTs, and HVDC.

Yilu Liu (S'88–M'89–SM'99–F'04) received the B.S. degree from Xi'an Jiaotong University, Xi'an, China, and the M.S. and Ph.D. degrees from Ohio State University, Columbus, in 1986 and 1989, respectively.

She is currently the Governor's Chair Professor with the Department of Electrical Engineering and Computer Science, University of Tennessee/Oak Ridge National Laboratory (ORNL). She leads the effort to establish a nationwide power frequency dynamic monitoring network, which is now operated at UTK and ORNL as GridEye. Her current research interests include power system wide-area monitoring and control, large interconnection level dynamic simulations, electromagnetic transient analysis, and power transformer modeling and diagnosis.

Wei Gao (M'05) received the B.E. degree in electrical engineering from the University of Science and Technology of China in 2005, and the Ph.D. degree in computer science from Pennsylvania State University in 2012. He is currently an Assistant Professor with the Department of Electrical Engineering and Computer Science, University of Tennessee, Knoxville. His research interests include wireless and mobile network systems, mobile cloud computing, mobile social networks, and cyber-physical systems.